# A 3-D Microscale Model for $CO_2$ Gas Transport in Tomato Leaves during Photosynthesis

Q.T. Ho, P. Verboven, E. Herremans,
M.A. Retta, T. Defraeye and B.M. Nicolaï
Flanders Center of Postharvest Technology
BIOSYST-MeBioS
Katholieke Universiteit Leuven
Willem de Croylaan 42, B-3001 Leuven
Belgium

Xinyou Yin, R.K. Thapa and P.C. Struik
Centre for Crop Systems Analysis
Wageningen University
P.O. Box 430, 6700 AK Wageningen
The Netherlands

**Keywords:** biophysical model, biochemical model, gas diffusion, mesophyll conductance

## Abstract

**Exchange of $CO_2$ in tomato (*Solanum lycopersicum* L.) leaves was modelled using combined gas diffusion and photosynthesis kinetics in a real 3-D geometric representation of the cellular microstructure, obtained by synchrotron radiation X-ray microtomography. The microscale model for gas exchange accounted for diffusive mass transport of $CO_2$ in the intercellular space (pores), the cell wall network and the intracellular liquid of cells. The photosynthesis kinetics described by the extended Farquhar, von Caemmerer & Berry model were coupled to the gas exchange inside the mesophyll cells. The coupled model was validated by means of gas exchange and chlorophyll fluorescence measurements. The model provides detailed insight into the mechanisms of gas exchange and insight into the effects of changes in ambient $CO_2$ concentration or photon flux density on stomatal and mesophyll conductance. The resistance to diffusion of $CO_2$ from the intercellular air spaces within the leaf through the mesophyll to the sites of carboxylation during photosynthesis depended on the 3-D microstructure of leaf tissue. The model represents an important step forward to study $CO_2$ diffusion coupled to photosynthesis at the leaf tissue level, taking into account its actual 3-D microstructure.**

## INTRODUCTION

Photosynthesis is amongst the most important metabolic processes in plants. During photosynthesis, $CO_2$ diffuses from the atmosphere into the leaf and finally to the site of carboxylation in the chloroplast stroma (Flexas et al., 2007). The diffusion of $CO_2$ through the leaves has been shown to be impeded by several conductances such as the regulation of the opening of the stomata and conductive properties of the mesophyll (Evans et al., 2009). The stomatal conductance ($g_s$) determines the gas exchange from the phyllosphere into the intercellular air space (von Caemmerer and Farquhar, 1981). The mesophyll conductance ($g_m$) is defined as the conductance for the transfer of $CO_2$ from the intercellular air space ($C_i$) to the site of carboxylation in the mesophyll cells ($C_c$). Correlations of the conductances with leaf structural properties have not always been clear (Flexas et al., 2007). Both $g_s$ as well as $g_m$ are apparent variables rather than physical constants as they implicitly incorporate microstructural and biochemical features of the tissue, cells and organelles that are involved in the gas transport mechanism.

Here, we describe a microscale model for $CO_2$ exchange through the leaf by coupling a biophysical model of gas diffusion to the biochemical model of photosynthesis. The diffusion model accounted for mass transport of $CO_2$ in the intercellular space (pores), the cell wall network and the intracellular liquid of cells. The photosynthetic kinetics described by the extended Farquhar, von Caemmerer & Berry (FvCB, Farquhar et al., 1980) model was incorporated into the gas transport equations. The model can be used to quantify the importance of the different pathways of gas exchange, and to analyze the response of the net photosynthesis $A$ and conductance $g_m$ to environmental factors such as $CO_2$ and irradiance. Tomato (*Solanum lycopersicum* L.)

leaf was chosen as the model system.

## MATERIALS AND METHODS

### Photosynthetic Kinetics Model

The FvCB model was used in this study to describe the gross $CO_2$ fixation rate $A_G$ in the chloroplasts of tomato plants (Farquhar et al., 1980; von Caemmerer, 2000). Briefly,

$$A_G = \min(A_{G,c}, A_{G,j}, A_{G,p}) \tag{1}$$

where $A_{G,c}$ = the Rubisco-limited rate, $A_{G,j}$ = the RuBP(Ribulose-1,5-bisphosphate) regeneration or electron transport limited rate, and $A_{G,p}$ = the triose phosphate utilization (TPU) limited rate of $CO_2$ assimilation. $A_{G,c}$, $A_{G,j}$ and $A_{G,p}$ were calculated from

$$A_{G,c} = \frac{(C_c - \Gamma^*)V_{c,max}}{C_c + K_{m,C}(1 + O_2 / K_{m,O_2})} \tag{2}$$

$$A_{G,j} = \frac{(C_c - \Gamma^*)J}{4C_c + 8\Gamma^*} \tag{3}$$

$$A_{G,p} = 3T_p \tag{4}$$

where $C_c$ and $O_2$ are the $CO_2$ and $O_2$ concentration in the chloroplast, respectively; $J$ is the rate of electron transport; $T_p$ is the rate of triose phosphate export from the chloroplast; and $\Gamma^*$ is the $CO_2$ compensation point in the absence of respiration. $K_{m,C}$, $K_{m,O2}$ and $V_{c,max}$ are constants of Rubisco activity-limited carboxylation. The net photosynthesis rate $A$ was defined as $A = A_G - R_d$, where $R_d$ is the respiratory $CO_2$ release other than by photorespiration. For further details, refer to Yin et al. (2009).

### Gas Exchange and Chlorophyll Fluorescence Measurements

'Admiro' cultivar was used for photosynthesis measurements. Plants were grown under natural plus supplemental light and the photoperiod was 16 hours per day. Simultaneous gas exchange and chlorophyll fluorescence measurements at both 21% and 2% $O_2$ were performed at the beginning of the flowering stage, using an open gas exchange system (Li-Cor 6400; Li-Cor Inc, Lincoln, NE, USA) and an integrated fluorescence chamber head (LI-6400-40; Li-Cor Inc, Lincoln, NE, USA). Measurements were carried out on four plants; we selected the distal-side leaflets from the top-most fully expanded leaf and from the fourth leaf below the top-most fully grown leaf for measurements. All measurements were made at a leaf temperature of 25°C and a leaf-to-air vapour pressure difference of 1.0-1.6 kPa. For the $C_i$ (intercellular $CO_2$ partial pressure) response curves, the ambient air $CO_2$ concentration ($C_a$) was increased step-wise: 50, 100, 150, 200, 250, 350, 500, 650, 1000, and 1500 μmol $mol^{-1}$, while keeping incident irradiance $I_{inc}$ at 1000 μmol $m^{-2}$ $s^{-1}$. For the $I_{inc}$ response curves, the photon flux densities were in a series: 0, 20, 65, 100, 150, 200, 500, 1000, 1500, 2000 μmol $m^{-2}$ $s^{-1}$, while keeping $C_a$ at 380 μmol $mol^{-1}$ for measurements at 21% $O_2$, and keeping $C_a$ at 1000 μmol $mol^{-1}$ for measurements at 2% $O_2$ to ensure a non-photorespiration condition. The photosynthetic parameters of the FvCB model were estimated using method described by Yin et al. (2009) and are given in Table 1.

### Microscale Gas Exchange Model

Microscale diffusion was assumed to dominate transport in each of the pores and cells, while in the chloroplasts, photosynthesis was assumed to take place. Microscale diffusion in air pores and cells can be described by:

$$\frac{\partial C_{CO2,i}}{\partial t} = \nabla \cdot D_{CO2,i} \nabla C_{CO2,i} - \frac{A}{d \cdot f_c} + \frac{R_d}{d \cdot f_m} + B \tag{5}$$

$$\frac{\partial C_{HCO_3^-,c}}{\partial t} = \nabla \cdot D_{HCO_3^-,c} \nabla C_{HCO_3^-,c} - B \quad (6)$$

where the index $i$ indicates the gas phase of the pores ($g$) or the liquid phase of the cells ($l$). $C_{CO2,i}$ (mol m$^{-3}$) is the $O_2$ concentration in phase $i$, $\nabla$ is the gradient operator (m$^{-1}$) and $D_{CO2,i}$ (m$^2$ s$^{-1}$) is the $CO_2$ diffusivity in phase $i$, $d$ (m) is the leaf thickness while $f_c$ and $f_m$ are the fractions of chloroplasts and cytosols of the leaf, respectively. The second term in Equation (5) is the volumetric $CO_2$ consumption by photosynthesis (described by the FvCB model) in the chloroplasts while the third term is the volumetric $CO_2$ production by respiration of mitochondria in the cytoplasm. The last term of Equations (5) and (6) is the net hydration rate of $CO_2$ to $HCO_3^-$:

$$B = k_2 \frac{[H]^+ C_{HCO_3^-,c}}{K} - k_1 C_c \quad (7)$$

where $k_1$, $k_2$ and $K$ are the rate constants of the $CO_2$ to $HCO_3^-$ conversion (for further details see Ho et al., 2011). The relationship between the equilibrium $CO_2$ concentration in the gas and liquid phase was assumed to be described by Henry's law. The resistance to the gas transport of the cell wall and cell membrane was taken into account at the interface between gas and liquid phase. Values of the physical properties that appear in the microscale model are given in Table 2.

**Leaf Microstructure**

The synchrotron X-ray computed tomography experiment of tomato (*Solanum lycopersicum*) leaves was performed at the European Synchrotron Radiation Facility in Grenoble, France. The 3-D microstructure of tomato leaf tissues were reconstructed from a series of slices of tomography images using Avizo image-processing software (Visualization Group Sciences). Further organelles inside the mesophyll cells were explicitly reconstructed. For simplicity, chloroplasts were modelled as a layer of 2.6 μm located beneath the boundary of the mesophyll cell. The vacuoles were modelled explicitly in the mesophyll cells by shrinking the cell volume by 70% and considering the shrunk volume to be vacuole. The layer between the chlorophyll layer and the tonoplast was considered to be cytoplasm.

**Numerical Solution**

The model for $CO_2$ diffusion was solved on the 3-D geometry using the finite volume method (Versteeg and Malalasekera, 1995). 3-D tomographic images of leaf tissue samples (127.5×127.5×195 μm) were discretized into $7.514\times10^6$ cube elements with axes of 0.75 μm. The model equations were discretized over the finite volume grid to yield a linear system of algebraic equations on the unknown concentrations at the nodes. The linear equation system was solved by the preconditioned conjugate gradient procedure available in Matlab (The Mathworks) on a 16-GB RAM node of the High-Performance Computer in the VSC – Flemish Supercomputer Center.

**RESULTS**

**Microscopic Gas Concentration Distribution**

The microscale model confirmed that there are indeed $CO_2$ gradients inside the leaf tissue. Figure 1 shows the simulation results of 3-D microscale $CO_2$ gas transport performed on tissue samples that were 164 μm thick (lower leaf) and 131 μm thick (upper leaf). Since the epidermis has a low permeability, transport of $CO_2$ occurred mostly through stomata. Tomato leaves have a large intercellular space (30-44%) and high connectivity resulted in a uniform $CO_2$ concentration of intercellular space. Clearly, the $CO_2$ concentration is low inside the cells. The chloroplasts were modelled as layers adhering to the mesophyll wall. $CO_2$ concentration gradient was found especially at the

sites where cells touch each other.

**Photosynthesis in Response to $CO_2$ Concentration**

In a next step, we investigated whether the microscale model was able to predict the measured response of leaf photosynthesis to the ambient $CO_2$ concentration in photorespiration conditions. Figures 2a and b show the results of the measured and simulated net photosynthesis rate at different intercellular $CO_2$ concentrations ($C_i$), photon flux density incident on leaves of 1000 μmol $m^{-2}$ $s^{-1}$ and 21% $O_2$. A good agreement was found between measured and simulated data. Both model and measured results predicted that the net photosynthesis of leaves rapidly increased at low $C_i$ concentrations but saturated at high $CO_2$ concentrations. In Figures 2c and d, the mesophyll conductance $g_m$ is plotted as a function of $C_i$. Excluding the low-$CO_2$ region where any assessment of $g_m$ is uncertain, clearly the measured mesophyll conductance decreased with increasing $CO_2$ levels. The modelled results indicated that mesophyll conductance also decreased with increasing $CO_2$ levels but then stabilized at high $CO_2$ concentrations.

**Photosynthesis of Upper and Lower Leaves**

Upper leaves and lower leaves are different in photosynthesis capacity and morphology characteristics. Synchrotron X-ray computed tomography experiments indicated that upper leaves were thinner than lower leaves. Mesophyll cells of upper leaves were smaller than those of lower leaves. Gas exchange and chlorophyll fluorescence measurements showed that the photosynthesis capacity of upper leaves was higher than that of lower leaves (Figs. 2a and b). Both simulations and measurements indicated that the mesophyll conductance of upper leaves was higher than that of the lower leaves (Table 3). A good agreement between the modelled and measured results was observed.

**DISCUSSION**

Several authors have used the reaction diffusion model to describe $CO_2$ uptake by leaves (Vesala et al., 1996; Aalto and Juurola, 2002). Such models were solved with geometrical simplifications, for example by assuming $CO_2$ diffusion through a single stomaton and the surrounding mesophyll using an axial symmetry model (Vesala et al., 1996), or by implementing a 3-D model for $CO_2$ gas exchange through the leaf but using basic geometrical elements such as spheres and cylinders representing mesophyll cells (Aalto and Juurola, 2002). While in the latter model the cells were separated by air gaps (Aalto and Juurola, 2002), in reality cells touch each other and this contact may reduce both the surface available for $CO_2$ exchange and the diffusion among the cells as we have clearly shown. The most realistic photosynthesis model to date was recently described by Tholen and Zhu (2011). Their model, while addressing 3-D $CO_2$ transport in a single mesophyll cell and incorporating subcellular features such as chloroplasts and mitochondria, does not account for any resistances due to the leaf microstructure and in particular the mesophyll. In this current model, we incorporated for the first time the actual microstructure as observed from synchrotron X-ray computed tomography experiments in the $CO_2$ transport model. This model confirmed the effect of mesophyll cells touching each other and thereby reducing the exchange surface between mesophyll and intercellular space. A large $CO_2$ gradient was found in the palisade mesophyll cells beneath the adaxial epidermis layer and contact surface between the mesophyll cells. Simulations with our model suggest that in tomato leaves, the actual microstructure indeed affects gas transport and mesophyll conductance in particular. Note that Tholen and Zhu (2011) did not address an important part of the gas exchange pathway – that from the ambient atmosphere through the stomata and the intercellular space towards the mesophyll cell.

The model predicted net photosynthesis similar to the measured values. The measured mesophyll conductance decreased with increasing $CO_2$ levels. The modelled

mesophyll conductance also decreased with increasing $CO_2$ levels but then stabilized at high $CO_2$ concentration. Note that the measured mesophyll conductance was estimated by assuming that the $CO_2$ assimilation was limited by the electron transport rate. However, the method using combined gas exchange and chlorophyll fluorescence data to estimate $CO_2$ concentration of chloroplast ($C_c$) and mesophyll conductance ($g_m$) may not be reliable at high ambient $CO_2$ concentration where most likely triosephosphate utilisation limits photosynthesis. On the other hand, a discrepancy of the mesophyll conductance at high $CO_2$ levels may indicate that some physiological processes related to photosynthesis are not incorporated in the model.

## CONCLUSIONS

Gas exchange in tomato leaves during photosynthesis was investigated by combining a microscale gas diffusion model with a model of photosynthetic kinetics. The combined model incorporated the actual 3-D tissue microstructure of the tomato leaf, which was derived from synchrotron X-ray computed images. The conductance of $CO_2$ from the intercellular airspaces within the leaf through the mesophyll to the sites of carboxylation during photosynthesis was dependent on the 3-D microstructure of leaf tissue. The upper leaves showed higher photosynthesis capacity and mesophyll conductance compared to the lower leaves. The model represents an important step forward to studing $CO_2$ diffusion coupled to photosynthesis at the leaf tissue level, taking into account its actual 3-D microstructure.

## ACKNOWLEDGEMENTS

The authors wish to thank the Research Council of the K.U. Leuven (OT 08/023), the Research Fund Flanders (project G.0603.08), and the Institute for the Promotion of Innovation by Science and Technology in Flanders (project IWT-050633) for financial support. Wageningen based authors have contributed to this work within the programme BioSolar Cells. Quang Tri Ho is a postdoctoral fellow of the Research Fund Flanders (FWO Vlaanderen).

## Literature Cited

Aalto, T. and Juurola, E. 2002. A three-dimensional model of $CO_2$ transport in airspaces and mesophyll cells of a silver birch leaf. Plant, Cell Environ. 25:1399-1409.

Bernacchi, C.J., Portis, A.R., Nakano, H., von Caemmerer, S. and Long, S.P. 2002. Temperature response of mesophyll conductance. Implications for the determination of Rubisco enzyme kinetics and for limitations to photosynthesis in vivo. Plant Physiol. 130:1992-1998.

Einstein, A. 1905. On the movement of small particles suspended in stationary liquids required by the molecular-kinetic theory of heat. Ann. Phys. 17:549-560.

Evans, J.R, Kaldenhoff, R., Genty, B. and Terashima, I. 2009. Resistances along the $CO_2$ diffusion pathway inside leaves. J. Exp. Bot. 60:2235-2248.

Farquhar, G.D., von Caemmerer, S. and Berry, J.A. 1980. A biochemical model of photosynthetic $CO_2$ assimilation in leaves of $C_3$ species. Planta 149:78-90.

Flexas, J., Diaz-Espejo, A., Galmes, J., Kaldenhoff, R., Medrano, H. and Ribas-Carbó, M. 2007. Rapid variation of mesophyll conductance in response to changes in $CO_2$ concentration around leaves. Plant, Cell Environ. 30:1284-1298.

Frost-Christensen, H. and Floto, F. 2007. Resistance to $CO_2$ diffusion in cuticular membranes of amphibious plants and the implication for $CO_2$ acquisition. Plant, Cell Environ. 30:12-18.

Geers, C. and Gros, G. 2000. Carbon dioxide transport and carbonic anhydrase in blood and muscle. Physiol. Rev. 80:681-715.

Gutknecht, J., Bisson, M.A. and Tosteson, F.C. 1977. Diffusion of carbon dioxide through lipid bilayer membranes: effect of carbonic anhydrase, bicarbonate, and unstirred layers. J. Gen. Physiol. 69:779-794.

Ho, Q.T., Verboven, P., Verlinden, B.E., Herremans, E., Wevers, M., Carmeliet, J. and

Nicolaï, B.M. 2011. A 3-D multiscale model for gas exchange in fruit. Plant Physiol. 155:1158-1168.
Jolly, W.L. 1985. Modern Inorganic Chemistry. McGraw-Hill, New York.
Lide, D.R. 1999. Handbook of Chemistry and Physics. CRC Press, New York.
Tholen, D. and Zhu, X.G. 2011. The mechanistic basis of internal conductance: a theoretical analysis of mesophyll cell photosynthesis and $CO_2$ diffusion. Plant Physiol. 156:90-105.
Versteeg, J.K. and Malalasekera, W. 1995. An Introduction to Computational Fluid Dynamics. Longman Scientific & Technical, Harlow, UK.
Vesala, T., Ahonen, T., Hari, P., Krissinel, E. and Shokhirev, N. 1996. Analysis of stomatal $CO_2$ uptake by a three-dimensional cylindrically symmetric model. New Phytol. 132:235-245.
von Caemmerer, S. 2000. Biochemical Models of Leaf Photosynthesis. Techniques in Plant Sciences No. 2. CSIRO Publishing, Collingwood, Victoria, Australia.
von Caemmerer, S. and Farquhar, G.D. 1981. Some relationships between the biochemistry of photosynthesis and the gas-exchange of leaves. Planta 153:376-387.
Yin, X., Struik, P.C., Romero, P., Harbinson, J., Evers, J.B., Van Der Putten, P.E.L. and Vos, J. 2009. Using combined measurements of gas exchange and chlorophyll fluorescence to estimate parameters of a biochemical $C_3$ photosynthesis model: A critical appraisal and a new integrated approach applied to leaves in a wheat (*Triticum aestivum*) canopy. Plant, Cell Environ. 32:448-464.

## Tables

Table 1. Values (± standard error of estimate if applicable) of photosynthetic parameters estimated for 'Admiro' tomato leaves.

| Parameters | Upper leaves | Lower leaves |
|---|---|---|
| $V_{c,max}$ (µmol $m^{-2}$ $s^{-1}$) | 133.6±13.68 | 57.94±3.08 |
| $K_{m,C}$ (µbar) * | 267 | 267 |
| $K_{m,O}$ (mbar) * | 164 | 164 |
| $S$ | 0.473 | 0.429 |
| $\Gamma$* (µbar) | 33.52 | 33.52 |
| $R_d$ -common (µmol $m^{-2}$ $s^{-1}$) | 1.784 | 0.933 |
| $R_{dk}$ (µmol $m^{-2}$ $s^{-1}$) | 2.611 | 2.431 |
| $T_p$ (µmol $m^{-2}$ $s^{-1}$) | 9.04±0.30 | 8.1 |

*Value is given by Bernacchi et al. (2002).

Table 2. Physical parameters of the microscale gas exchange model. Diffusion in the liquid phase was assumed to follow the Stokes-Einstein law (inversely related to the kinematic viscosity of the solvent, Einstein, 1905), $D_{CO2,l} = D_{CO2,water}/\eta$.

| Model parameters | Symbol | Values |
|---|---|---|
| Diffusivity | | |
| - Pore | $D_{CO2,g}$ | $1.60\times10^{-5}$ m$^2$ s$^{-1}$ at 20°C [a] |
| - Cell | $D_{CO2,water}$ | $1.67\times10^{-9}$ m$^2$ s$^{-1}$ at 20°C [a] |
| | $D_{HCO_3^-,c}$ | $1.17\times10^{-9}$ m$^2$ s$^{-1}$ [b] |
| Cuticular membrane permeability | $P_{cuti}$ | $7\times10^{-6}$ m s$^{-1}$ [c] |
| Cellular membrane permeability | $P_{mem}$ | $3.5\times10^{-3}$ ms$^{-1}$ [d] |
| Henry's constant | $H$ | 0.83 (mol m$^{-3}$ liquid)(mol m$^{-3}$ gas)$^{-1}$ at 25°C [a] |
| $CO_2$ reaction rate constants | $k_1$ | 0.039 s$^{-1}$ [e] |
| | $k_2$ | 23 s$^{-1}$ [e] |
| | $K$ | $2.5\times10^{-4}$ mol L$^{-1}$ [e] |
| Cytosol viscosity | $\eta$ | 2 (relative to water) [f] |
| Stroma viscosity | $\eta$ | 2 (relative to water) |

[a]Lide (1999), [b]Frost-Christensen and Floto (2007), [c]Geers and Gros (2000), [d]Gutknecht et al. (1977), [e]Jolly (1985), and [f] Tholen and Zhu (2011).

Table 3. Mesophyll conductance ($g_m$) calculated from measurement and simulation. $R_d$ and $R_{dk}$ are day respiration and dark respiration (further details are described by Yin et al., 2009). From combined gas exchange and chlorophyll measurements, mesophyll conductance was calculated with different $R_d$ -common and $R_{dk}$.

| | $R_d$ | $C_a$ | $g_m$ (mol m$^{-2}$ s$^{-1}$) | |
|---|---|---|---|---|
| | | (μmol mol$^{-1}$) | Lower leaves | Upper leaves |
| Measurement | $R_d$-common | 350 | 0.120 | 0.183 |
| | $R_{dk}$ | 350 | 0.158 | 0.204 |
| Simulation | $R_d$-common | 350 | 0.161 | 0.214 |
| | $R_{dk}$ | 350 | 0.161 | 0.213 |

## Figures

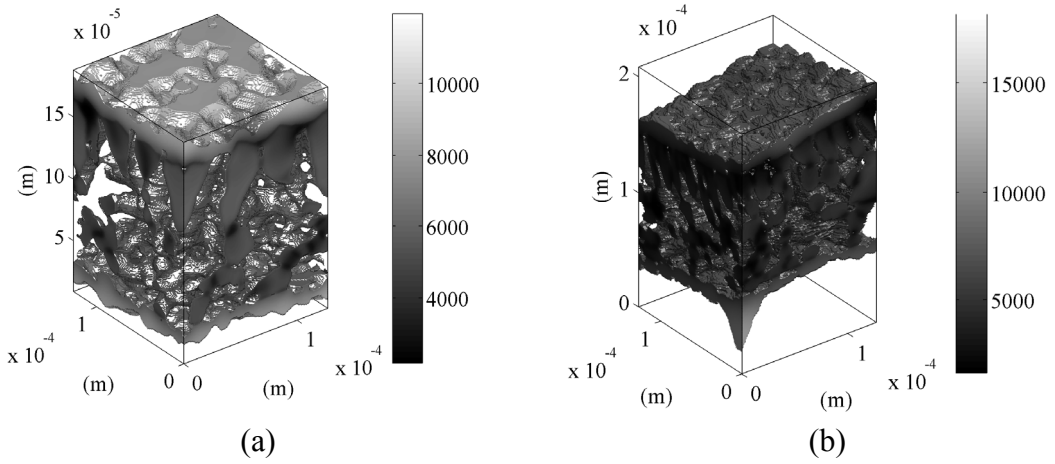


Fig. 1. Computed intra cellular $CO_2$ distribution in a tomato leaf ('Admiro'). The ambient conditions were 350 µmol $mol^{-1}$ $CO_2$, 21% $O_2$, photon flux density incident irradiance ($I_{inc}$) of 1000 µmol $m^{-2}$ $s^{-1}$ and 25°C. Concentrations are expressed in µmol $m^{-3}$. (a) and (b) are upper and lower leaves, respectively.

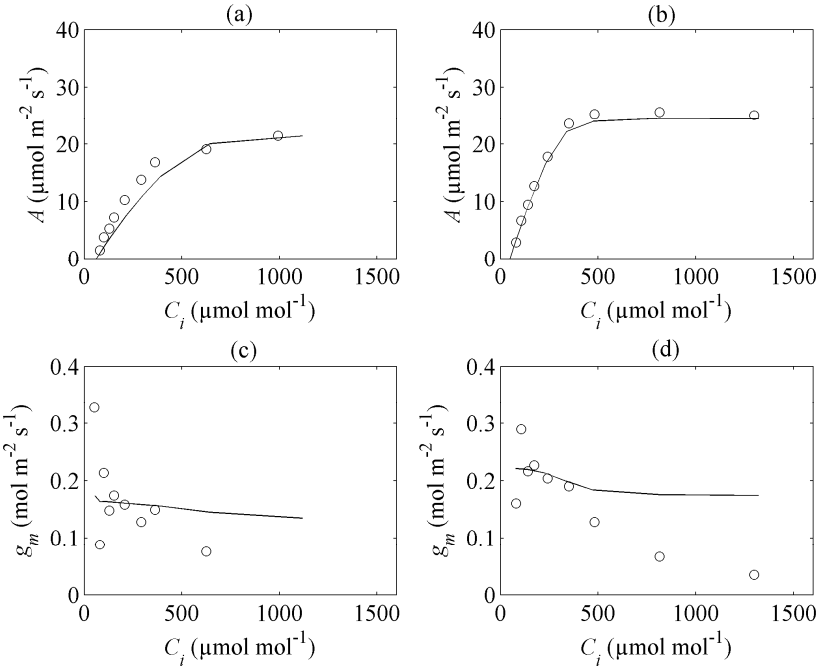


Fig. 2. Simulations and measurements of photosynthesis of tomato 'Admiro' leaves at different conditions of intercellular $CO_2$ concentration $C_i$ at 21% $O_2$, photon flux density incident to leaves $I_{inc}$ of 1000 µmol $m^{-2}$ $s^{-1}$ and 25°C. Panels (a) and (b) show net photosynthesis $A$ as function of $C_i$ of upper and lower leaves, respectively. Panels (c) and (d) show mesophyll conductance $g_m$ as function of $C_i$ for upper and lower leaves. The symbols represent measurements while the lines indicate model predictions.